Composite Structures 256 (2021) 113101

Contents lists available at ScienceDirect

Composite Structures

journal homepage: www.elsevier.com/locate/compstruct

Modeling and experimental validation of compaction pressure distribution for automated fiber placement

Junxia Jiang, Yuxiao He *, Han Wang, Yinglin Ke

State Key Laboratory of Fluid Power and Mechatronic Systems, School of Mechanical Engineering, Zhejiang University, Hangzhou, China
Key Laboratory of Advanced Manufacturing Technology of Zhejiang Province, School of Mechanical Engineering, Zhejiang University, Hangzhou, China

ARTICLE INFO

Keywords:
Automated fiber placement
Compaction pressure distribution
Deformation analysis
Numeral calculation

ABSTRACT

Automated fiber placement is especially suitable for manufacturing composite components with curved surfaces, in which case the uneven compaction pressure distribution is an important factor affecting layup quality, but it has not been widely explored. In this paper, a theoretical model of the compaction pressure distribution for layup on irregular curved surface is established by analyzing the contact between the compaction roller and prepreg layers. Based on the model, a numerical algorithm for calculating the pressure distribution in the whole placement process is proposed. Then the pressure distribution around four path points of a winglet mold is obtained and validated by the subsequent experiment. The results show that the model can be used to predict the compaction pressure distribution before the placement and analyze the layup quality and defects from the perspective of compaction pressure.

1. Introduction

Advanced composite materials have been widely used in aerospace industry and other fields due to their high specific strength, specific modulus and significant weight reduction [1,2]. Automatic fiber placement (AFP) is an important technology for manufacturing advanced composite components. During AFP, each slit-tape is driven individually and laid onto a mold or previous layers under a controlled tension by a moving AFP head, which consists of a heater and a compaction roller [3,4], as shown in Fig. 1. The compaction roller, whose main role is providing a required compaction force and reducing the voids between layers [3,5], is mainly composed of a shaft, a sleeve, two bearings and a rubber cover.

Compaction force is one of the most important process parameters for AFP. It is known that increasing compaction force within a certain range can improve prepreg tack levels and layup quality, and reduce layup defects such as wrinkles and bridgings [5–9]. And for thermoplastic prepreg, increasing compaction force helps to reduce void content and improve the mechanical properties of the final laminates [10–13].

However, what affects the layup quality in essence is the compaction pressure (unit: Pa), the compaction force (unit: N) on unit area. Most researches used the force as the process parameter because these researches performed on flat molds, in which case the pressure is relatively uniform. But most molds in aerospace industry have irregular curved surfaces, and layup onto curved surface is the case where AFP is mostly used. The axial deformation of the compaction roller will be uneven, resulting in an uneven pressure distribution, which leads to uneven tack levels and may even cause defects such as tow bridges, wrinkles and bubbles [14–16]. However, the use of compaction force alone cannot describe the phenomenon of uneven pressure and the formation of defects. In addition, the compaction force needs to be matched with the structural size and hardness of the compaction roller, otherwise the tack levels will be different even if the force is the same. Thus, it is necessary to study the compaction pressure distribution, which has not been widely explored.

Cheng et al. [17] studied the contact characteristic between the compaction roller and prepreg layers and established a deformation model to obtain the morphology change of the prepreg. Bakhshi and Hojjati [5] preformed a series of AFP trials at various process conditions with different compaction rollers, and concluded that sufficient and uniform pressure helps to reduce the number of wrinkles and blisters. Sonmez and Hahn [18] modeled the relationship between process parameters and the quality of thermoplastic laminates. They considered that as reducing roller diameter, the interlaminar stress become more concentrated, and small roller sizes are not conducive to bonding. Jiang et al. [19] studied the compaction pressure distribution by finite element simulation and experimental verification. They con-

* Corresponding author at: State Key Laboratory of Fluid Power and Mechatronic Systems, School of Mechanical Engineering, Zhejiang University, Hangzhou, China.
E-mail address: yuxiaohe@zju.edu.cn (Y. He).

https://doi.org/10.1016/j.compstruct.2020.113101
Received 8 February 2020; Revised 23 June 2020; Accepted 4 October 2020
Available online 10 October 2020

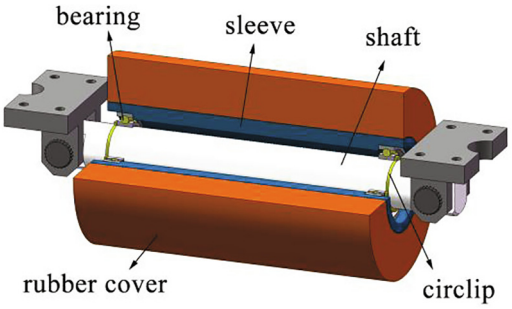

Fig. 1. The compaction roller for AFP.

cluded that the pressure uniformity can be improved by optimizing the roller structure: reducing the hardness and length and increasing the diameter of compaction roller. Hertz theory [20] can be used to analyze the contact of elastic solids, but it is based on infinitesimal deformation assumption and not suitable for the deformation analysis of the rubber compaction roller. To our knowledge, there is no paper focused on theoretical calculation of the compaction pressure distribution for automated fiber placement.

In this paper, a theoretical model of compaction pressure distribution for layup onto irregular curved surface is established by analyzing the contact deformation and contact stress between the roller and prepreg layers at any path point. Two parameters in the model are fitted by finite element method (FEM). And the time-dependent through-thickness modulus of prepreg is obtained from compaction test. Based on the model, a numerical algorithm is further proposed for calculating the pressure distribution in the whole placement process. After that, the theoretical pressure distribution around four path points of a winglet mold is obtained. Finally, in order to validate the model, pressure distribution measurement experiment was carried out by using pressure measurement film. The results show that the compaction pressure distribution can be predicted with this model. Moreover, the model provides a basis for analyzing layup defects, selecting appropriate compaction rollers and determining the number of slit-tapes before the placement.

2. Modeling of the compaction pressure distribution

The compaction pressure of AFP is essentially the contact pressure between the roller and prepreg layers. However, it is relatively difficult to get an accurate solution. Firstly, most composite components suitable for AFP have irregular complex curved surfaces. Some areas are concave and some are convex, and there is no function expression for such surfaces. Besides, the layers surface is uneven because of the existence of layup defects such as gaps, overlaps and wrinkles. Moreover, the rubber cover of the compaction roller exhibits large deformation after being pressed, in which case the differential equation of equilibrium and the geometrical equation of elasticity are not applicable. Thus, we made the following basic simplifications to obtain an approximate solution for the compaction pressure distribution.

(i) The rolling of the roller causes prepreg and roller to be subjected to tangential friction. The main effect of the friction is to cause tangential deformation of the roller and prepreg. For prepreg, the modulus in fiber direction is about four orders of magnitude higher than that in thickness direction. Thus, the tangential deformation of prepreg caused by friction is relatively small. And for the roller, friction causes the contact center slightly lags behind the roller axis (about 0–3.5 mm). Thus, due to the main concern about compaction pressure distribution, the effect of friction is simplified as the actual contact center lags behind the target path point.

(ii) The contact zone of the roller and layers is generally strip-shaped. Then the three-dimensional strain problem is simplified as a plane strain one, ignoring the axial deformation of the roller.

2.1. Contact analysis between the compaction roller and prepreg layers for layup onto irregular curved mold surface

During the layup process, the position and pose of the roller coordinate system $\{O_H\}$ and the path point coordinate system $\{O_{Pj}\}$ will be the same with respect to the machine coordinate system $\{O_{Base}\}$, as shown in Fig. 2(a) and Eq. (1). And the four coordinates are known from the trajectory planning and inverse kinematics.

$$\begin{cases} {}^{Base}T_{P_j} = {}^{Base}T_M^M T_{P_j} \\ {}^{Base}T_H = {}^{Base}T_{P_j} \end{cases}, \ j = 1, 2, \cdots, n \tag{1}$$

where ${}^{X}\boldsymbol{T}_{Y}$ represents the position and pose of the coordinate system $\{O_Y\}$ relative to the coordinate system $\{O_X\}$. $\{O_M\}$ is the mold coordinate system.

Take any path point P_j on any path l for analysis (see Fig. 2(b)). Contact center P_j' between compaction roller and prepreg layers lags behind P_j by Δl due to friction, and P_j' is also on path l. $\Delta l = |P_jP_j'|$, and its value is generally 0–3.5 mm according to the structural parameters of the roller and the value of compaction force. The spatial rectangular coordinate system $\{O(P_j')\}$ is set as follows: the origin O is at P_j', x is the tangential direction along l, y is the geodesic curvature direction of l, and z is the normal direction of the layers surface at point O. The axis of compaction roller is parallel to y-axis. L is the length of the compaction roller. Σ is the contact zone between the roller and the layers surface. Take any cross section $y = y_a$ parallel to xOz plane to analyze the contact, and $y_a \in [-L/2, L/2]$.

As illustrated in Fig. 2(c), F is the compaction force applied at target path point P_j, and F is parallel to the normal direction of layers surface at P_j'. The angle between F and z-axis is γ. The pressure distribution around point P_j in the rolling state of the roller is simplified as pressure distribution around P_j' in the static state, in order to correct for the effect of the friction. r is the inner radius of the rubber cover and R is the outer radius. S_m is the irregular curved mold surface and it is known. S and h are the layers surface and thickness before the contact, respectively. S can be obtained by thickening S_m by h, where $h = nh_0$, n is the number of layers, and h_0 is the thickness of a single prepreg layer. After applying F, the layers surface S is deformed to S'. Since the rigidity of the mold and the sleeve is relatively large, they are taken as rigid bodies.

For the moment, assume the shape of the roller remains as an arc after the deformation. Take any point A on the original surface of the roller for analysis. After the deformation, A moves to $A'(x, y_a, z)$ along the radius direction, and A' is on S'. $d(x, y_a, z)$ is the distance between A' and the roller axis. Then the compressive strain $\varepsilon(x, y_a, z)$ and the resultant stress $\sigma(x, y_a, z)$ of the roller at A' are obtained as follows:

$$\begin{cases} \varepsilon(x, y_a, z) = \frac{R - d(x, y_a, z)}{R - r} \\ \sigma(x, y_a, z) = \frac{E_C \varepsilon(x, y_a, z)}{1 - \varepsilon(x, y_a, z)} \end{cases} \tag{2}$$

where E_C is the effective compression modulus and $E_C = E(A + BS^n)$ [21]. E is the Young's modulus of elasticity and $n = 2$ for natural rubber. A, B and S are constants related to the stressed area, hardness and shape of the material, but their values are difficult to estimated for the cylindrical roller. Thus, the value of E_C is to be determined by other methods, which is given in Section 2.2.

The projection of σ on the normal direction of S' is the contact pressure $p(x, y_a, z)$, which is exactly the compaction pressure need to be obtained, as shown in Eq. (3). And $\sigma_z(x, y_a, z)$, the projection of σ on z-axis, can also be obtained.

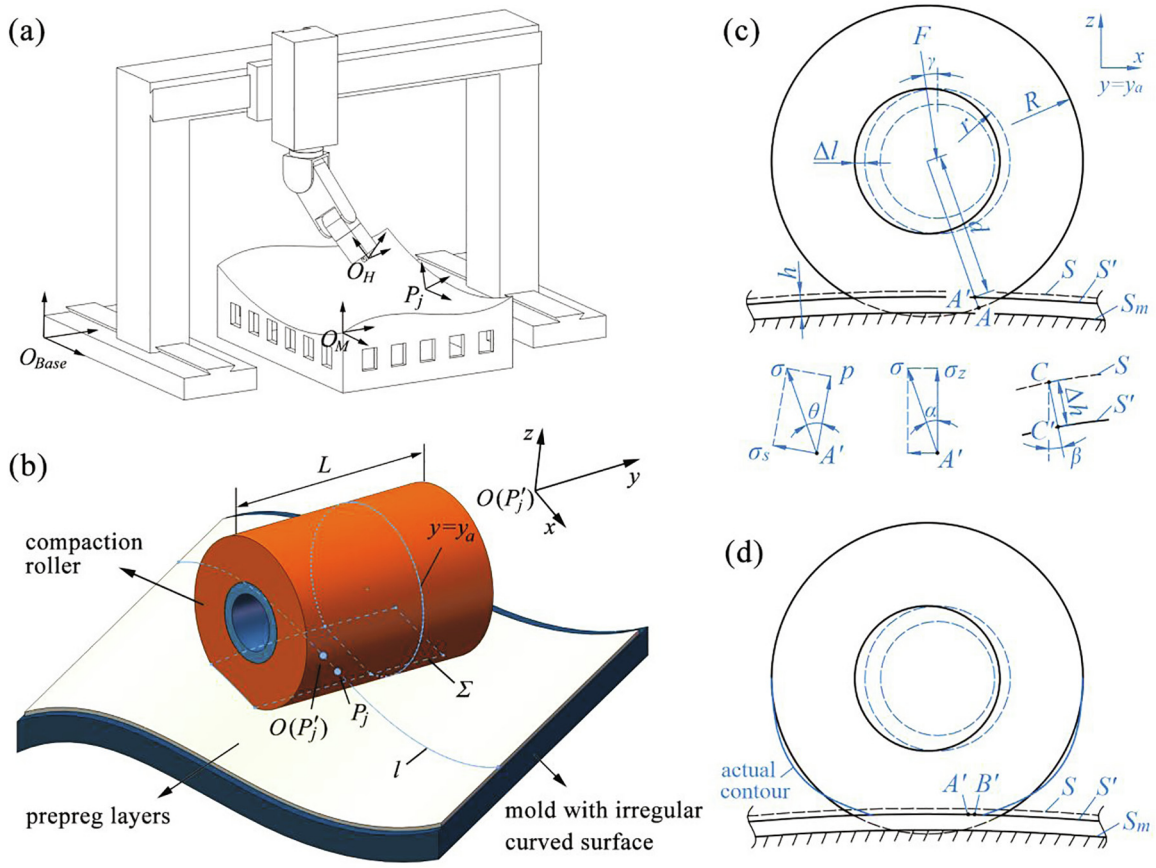

Fig. 2. (a) The four coordinate systems in AFP; (b) the static contact between the compaction roller and the prepreg layers at any path point P_j; (c) the deformation and the stress of the roller and layers in cross section $y = y_a$; (d) the actual contour of the roller after the deformation.

$$\begin{cases} p(x,y_a,z) = \sigma(x,y_a,z)\cos[\theta(x,y_a,z)] \\ \sigma_z(x,y_a,z) = \sigma(x,y_a,z)\cos[\alpha(x,y_a,z)] \end{cases} \tag{3}$$

where $\theta(x, y_a, z)$ is the angle between σ and p, and $\alpha(x, y_a, z)$ is the angle between σ and z-axis. Integrate all $\sigma_z(x, y, z)$ over the total contact zone Σ and the result is equal to the component of compaction force F along z-axis, as shown in Eq. (4). Since the irregular surface S has no functional expression, the integral needs to be solved numerically (see Section 3).

$$\iint_{\Sigma} \sigma_z(x,y,z)\mathrm{d}S = F\cos\gamma \tag{4}$$

However, the actual contour of the roller after the deformation is not maintained as an arc, as shown in Fig. 2(d). In order to describe the change in contact width, a scaling factor k is introduced (the solution for k will be given in Section 2.2). The value of k also reflects the influence of friction on contact width. Firstly, select point $B'(x_k, y_a, z_k)$ on surface S', where $x_k = kx$. Point $B'(x_k, y_a, z_k)$ corresponds to point $A'(x, y_a, z)$. Secondly, calculate $p(x_k, y_a, z_k)$ and $\sigma_z(x_k, y_a, z_k)$ of B' using Eqs. (2)–(4), and substitute the value of $p(x_k, y_a, z_k)$ and $\sigma_z(x_k, y_a, z_k)$ into $p(x, y_a, z)$ and $\sigma_z(x, y_a, z)$ of A', respectively. Then Eqs. (2)–(4) are rewritten as follows:

$$\begin{cases} \varepsilon(x,y_a,z) = \frac{R-d(x_k,y_a,z_k)}{R-r} \\ p(x,y_a,z) = \frac{E_C\varepsilon(x_k,y_a,z_k)}{1-\varepsilon(x,y_a,z)}\cos[\theta(x_k,y_a,z_k)] \\ \iint_{\Sigma}\frac{E_C\varepsilon(x,y,z)}{1-\varepsilon(x,y,z)}\cos[\alpha(x_k,y,z_k)]\mathrm{d}S = F\cos\gamma \end{cases} \tag{5}$$

And for the deformation of the prepreg layers, $E_1 \gg E_3$ [22]. Besides, the external force on the layers is mainly the pressure in the direction of thickness. Due to the main concern about the pressure, only the out-plane deformation of prepreg is considered. Any point C (x_c, y_a, z_c) of surface S is deformed along the thickness direction to $C'(x_c', y_a', z_c')$ of surface S', as shown in Fig. 2(c). And the deformation $\Delta h(x_c, y_a, z_c)$ of the layers is given by:

$$\begin{cases} \Delta h(x_c,y_a,z_c) = E_3(t,T)hp(x_c,y_a,z_c) \\ x_c' = \begin{cases} x_c - \Delta h\sin[\beta(x_c,y_a,z_c)], \vec{t}\cdot\vec{i} \geqslant 0 \\ x_c + \Delta h\sin[\beta(x_c,y_a,z_c)], \vec{t}\cdot\vec{i} < 0 \end{cases} \\ y_a' = y_a \\ z_c' = z_c - \Delta h\cos[\beta(x_c,y_a,z_c)] \end{cases} \tag{6}$$

where $E_3(t,T)$ is the trough-thickness modulus of prepreg, which exhibits viscoelastic. t is the duration of the load, and T is the temperature. The test for measuring E_3 is shown in Section 2.3. β is the angle between the thickness direction and z-axis. $\vec{t}$ is the vector along the outer normal direction of S at point C, and $\vec{i}$ is the vector along x-axis. Thus, the correspondence between S' and S is established.

Combining equations (5) and (6), the compaction pressure distribution around each path point during the whole AFP process can be obtained. In the analysis, the shape of mold surface S_m is not limited and is stochastic, thus the model is suitable for general mold surfaces.

2.2. Solution for E_C and k

In Section 2.1, the values of the effective compression modulus E_C and the scaling factor k have not been determined. In this section, they are solved by finite element simulation and MATLAB function fitting.

A two-dimensional finite element model of compaction pressure distribution is created by ABAQUS/CAE. The mold created here is flat, which is the most basic case. The outer radius, inner radius and hardness of the rubber are $R = 40$ mm, $r = 20$ mm and $H = 35$ HA, respec-

tively. The element type of the rubber cover is set as CPE4RH and the rest parts CPE4R. The material parameters of each part are listed in Table 1. And in order to increase the calculation efficiency, the sleeve and the mold are constrained as "rigid body" due to their high modulus. Friction coefficient between outer surface of the roller and the mold surface is set as 0.357 [24]. Different forces 1 N–10 N are applied to the sleeve (the force applied means the compaction force on per unit length of the roller).

The simulation result is shown in Fig. 3(a). Take the contact center as the origin O, and the right as x-axis. According to the first two formulas of Eq. (5), a function of compaction pressure distribution in the case of flat mold is obtained, as shown in Eq. (7). Since the finite element model is two-dimensional and the mold is flat, p is a function only about x:

$$\begin{cases} \varepsilon(x) = \frac{R-\sqrt{d_0^2+(kx)^2}}{R-r} \\ p(x) = E_C \frac{\varepsilon(x)}{1-\varepsilon(x)} \frac{d_0}{\sqrt{d_0^2+(kx)^2}} \end{cases} \tag{7}$$

where d_0 is the distance between the roller center and the mold surface. From the simulation result, a set of contact pressure (CPRESS) p for a set of x coordinates is available. Thus, the unknowns in Eq. (7) are only E_C and k, and their values are then fitted using MATLAB. According to Fig. 3(b), the simulation result and the fitting result have general similarities, and the fitted values can be considered reasonable.

In addition, E_C and k are first of all functions of H, r and R. And as stated below Eq. (2), the value of E_C is related to the stressed area. Thus, define $\Delta d = R - d_0$, which is the maximum deformation of the compaction roller at each cross section y_a. Then E_C and k are also functions of Δd, that is, $E_C = E_C(\Delta d, H, r, R)$, $k = k(\Delta d, H, r, R)$. However, the specific function form is unknown. For the roller with specific structural parameters, in Eq. (5) E_C and k are rewritten as follows:

$$E_C = E_C(\Delta d),\ k = k(\Delta d) \tag{8}$$

The value of E_C and k under different compaction forces are listed in Table 2. When calculating compaction pressure distribution, obtain Δd for each section y_a and use the corresponding E_C and k. For other hardness and structural size of compaction roller, the same method can be used to obtain the corresponding E_C and k.

2.3. Measurement of $E_3(t,T)$

The time-independent mechanical properties E_3 is measured by compression test [25]. Layers were prepared from USN12500/7901 unidirectional carbon/epoxy prepreg, and the size was 40 mm long, 40 mm wide and 10 plies thick. The layers were firstly pressed under vacuum at room temperature for an hour before the test. The electronic universal testing machine UTM2503 used is shown in Fig. 4(a). In order to meet the temperature and time requirement of pressure measurement films in Section 4, E_3 under a load for 2 min at 25 °C is required. Thus, the two pressure plates of the universal testing machine were not heated. And a defined load of 160 N–960 N was applied, corresponding to compaction pressure of 0.1–0.6 MPa respectively. The load lasted for 3200 s, and the ambient temperature was kept at 25 °C. The results are shown in Fig. 4(b), and the value of E_3 at a load for 2 min are listed in Table 3.

Table 1
Material parameters of the sleeve, the mold and the rubber cover [23]

	E (MPa)	μ
The sleeve and the mold (steel)	2.1×10^5	0.3
The rubber cover (silicone rubber 35HA)	1.4	0.4995

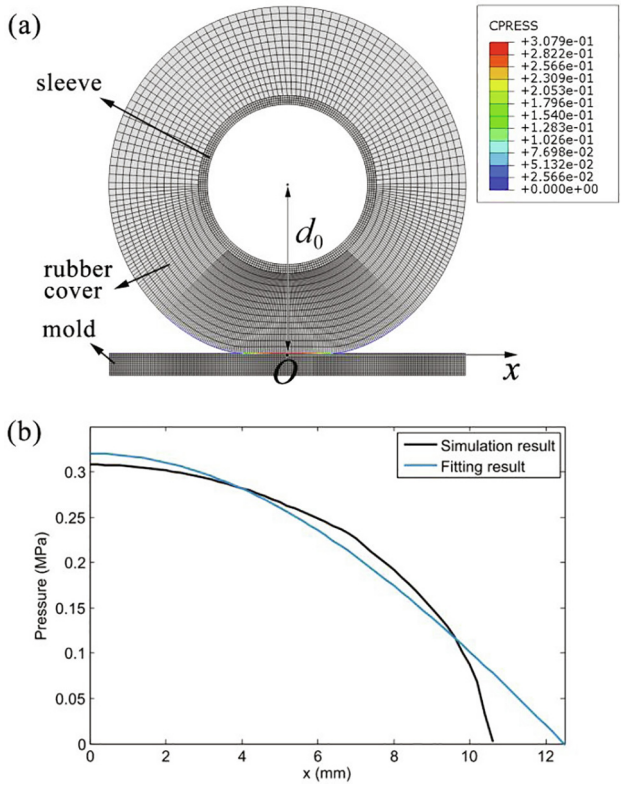

Fig. 3. (a) The simulation result of contact pressure (CPRESS) between the roller and flat mold (compaction force: 5 N/mm); (b) the simulation result and the fitting result of the compaction pressure distribution.

Table 2
The correspondence between E_C, k, F and Δd.

Compaction force (N/mm)	Δd (mm)	E_C (MPa)	k
1	0.6591	4.019	1.224
2	1.088	3.282	1.123
3	1.435	3.046	1.057
4	1.740	2.930	1.021
5	2.010	2.865	1.003
6	2.254	2.815	0.9803
7	2.480	2.772	0.9555
8	2.690	2.761	0.9541
9	2.888	2.744	0.9438
10	3.078	2.733	0.9385

3. Algorithm for the compaction pressure distribution

Since most molds for AFP have irregular surfaces with no function expression, the integral in the model cannot be calculated directly. Thus based on the model, a numerical algorithm for calculating compaction pressure distribution in the whole AFP process is proposed, as shown in Fig. 5.

The algorithm is then used to obtain the pressure distribution around four path points P_1, P_2, P_3, P_4 on the fifth prepreg layer of winglet mold of ARJ21 (see Fig. 6(a)). The distance Δl between P_1 and P_1' is set as 0 to meet the experimental requirements in Section 4. Thus, $\gamma = 0$. The through-thickness E_3 modulus of prepreg under different pressure is listed in Table 3. The thickness of a single slit-tape $h_0 = 0.125$ mm, thus the total thickness of the five layers $h = 0.625$ mm. By thickening the mold surface S_m by h, the fifth layers surface S_0 is obtained. The length of the compaction roller is 120 mm. r, R and H are 20 mm, 40 mm, and 35 HA, which are the same as that in Section 2.2. The compaction force is set to 600 N.

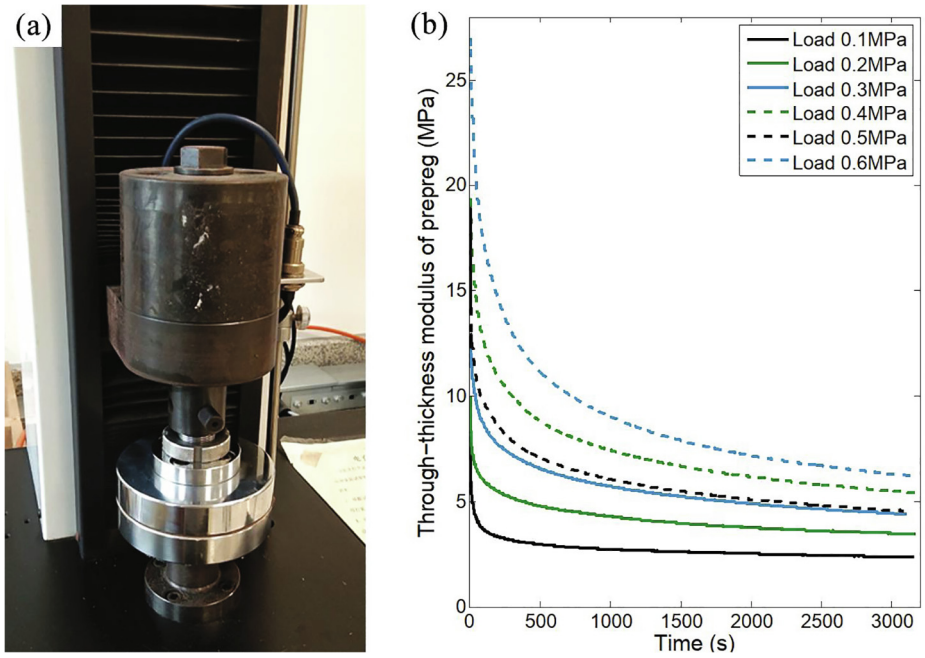

Fig. 4. (a) Experimental setup for compaction test; (b) curves of through-thickness modulus E_3 with time under defined loads at 25 °C.

Table 3
Through-thickness modulus E_3(2 min, 25 °C) of USN12500/7901 unidirectional carbon/epoxy prepreg (at ambient temperature of 25 °C under a load for 2 min).

Load (MPa)	0.1	0.2	0.3	0.4	0.5	0.6
E_3 (MPa)	3.58	5.88	8.39	12.17	9.47	16.65

In the following, the algorithm is explained by calculating the pressure distribution around point P_1. In Fig. 5, Step 1 is a preparation step, which aims to obtain the required inputs of the model: (i) the number of previous layers and the thickness of each layer; (ii) the coordinates of each path point P_j and offset path point P_j' relative to the mold; (iii) the tangential direction along the path at P_j', and the normal direction of the layers at P_j and P_j' (to determine x-axis, z-axis and γ); (iv) the points cloud of layers surface around P_j'; (v) the value of inner diameter, outer diameter, length, E_C and k of the compaction roller; (vi) the value of compaction force; (vii) the through-thickness modulus $E_3(t, T)$ of prepreg.

In Step 2, the initial relative position of the compaction roller and the layers surface S_0 is set as follows: the roller axis is parallel to y-axis, and the direction of the compaction force is parallel to z-axis. The initial distance c between the roller axis and the origin $O(P_1)$ is set as $(R + r)/2$. Then the surface needs to be discretized and then obtain the pressure at each discrete point numerically due to the irregular mold surface. In order to improve computational efficiency, the layers surface S_0 is cut appropriately around P_1', then a much smaller surface S is obtained. After that, discretize S to create point clouds $\{A_0\}$, as shown in Fig. 6(b) and 6(c).

In Step 3, combining bisection method, the compaction pressure around P_1 is calculated by Eqs. (5) and (6). e is the control accuracy, whose value is taken to be $F/100$. The deformation of the layers is calculated in Step 4, and the number of iterations is taken to be 3. And in Step 5, the compaction pressure distribution around P_1 is obtained, as shown in Fig. 6(d) and 7(a). It takes less than 4 s to calculate the pressure distribution around a path point. (The points cloud spacing is set to 1 mm, and the CPU of the computer used is AMD A10-5757 M 2.50 GHz.) Similarly, the pressure distribution around P_2, P_3 and P_4 can also be obtained by the algorithm, as illustrated in Fig. 7(b)(c)(d). By repeating this method, the compaction pressure distribution in the whole AFP process can be obtained.

4. Experimental validation

4.1. Experimental setup and materials

The experiment of compaction pressure distribution measurement was carried out to validate the model. Fig. 8(a) shows the 16-tow six-axis gantry AFP machine, developed by Zhejiang University. And Fig. 8(b) shows the winglet mold of ARJ21. The slit-tapes used was USN12500/7901 unidirectional carbon/epoxy prepreg with a width of 6.35 mm, supplied by Guangwei Composite, and the resin fraction is (33 ± 3) %. The parameters of the mold surface, compaction roller and slit-tapes are the same as that in Section 3.

In order to accurately measure the pressure distribution and contact zone, the pressure measurement film was used, which is provided by FUJIFILM Corporation. The film is composed of an A-Film and a C-Film, as shown in Fig. 8(c). The former is coated with a layer of microencapsulated color-forming material and the latter with a layer of color-developing material. They are positioned with the coated sides facing each other. When pressure is applied, the microcapsules in A-Film are broken, and the color-forming material reacts with the color-developing material and then red color appeared on C-Film.

The color density changes depending on the amount of pressure applied, which needs to be kept for 2 min to allows color-forming material to fully react with color-developing material. The thickness of A-Film and C-Film are both 0.1 mm, and the out surface is smooth. The pressure that can be accurately measured ranges from 0 to 0.6 MPa, and the temperature is required to be 20 ˚C ~ 35 ˚C.

FUJIFILM Corporation provides the calibration relationship between color density and pressure (see Fig. 8(d)). However, the color density is difficult to read, thus it needs to be converted into gray scale. Fit the relationship between the color sample density and gray scale, as depicted in Fig. 8(e). Combining Fig. 8(d) and (e), the corresponding relationship between the gray scale and the pressure can be obtained.

4.2. Experimental process and results

Five prepreg layers were pre-placed onto the mold surface, then the pressure measurement films were laid on the layers around the path points P_1, P_2, P_3, P_4. After that, the AFP head moved along the path l above the mold, stoped at the target path point and applied a static compaction force of 600 N onto the mold, as shown in Fig. 9(a). The force was parallel to the normal direction of the layers surface, and maintained for 2 min to be consistent with the pressure time in the calibration of the film. The heater of the AFP head was turned off in order to meet the temperature requirement of the film. In addition, the ambient temperature was kept at 25 ˚C with a relative humidity of (52 ± 3) %. Finally, the color density distribution on the films was obtained, as shown in Fig. 9(b)(c)(d)(e).

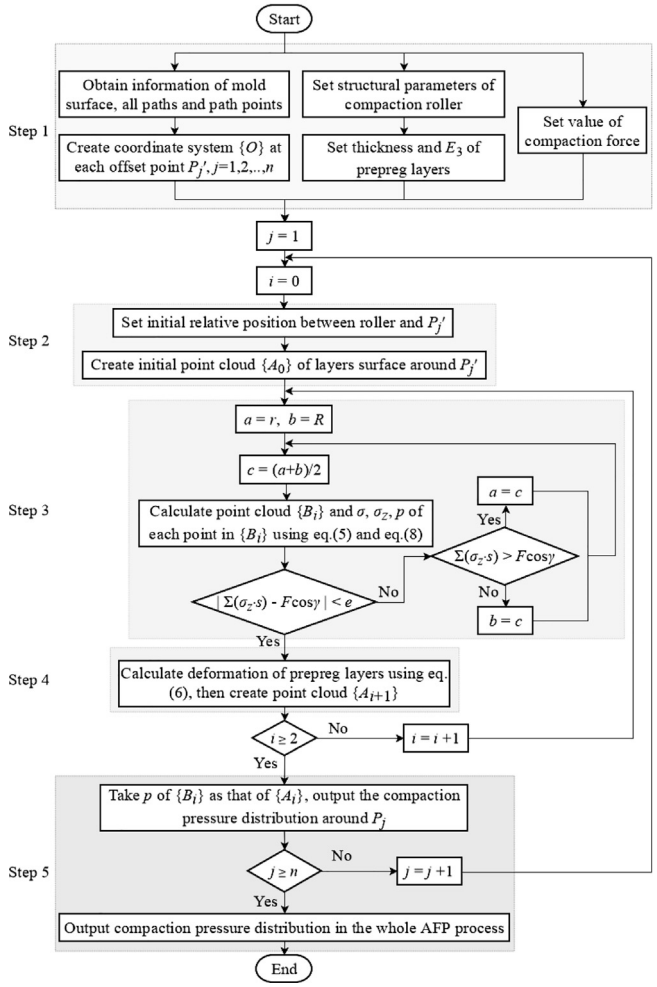

Fig. 5. Flow chart of the algorithm for compaction pressure distribution.

Fig. 9(b) – (e) was then converted into a gray scale figure, and then converted to compaction pressure distribution, as shown in Fig. 10. From the viewpoint of the contact area and the pressure distribution, the experimental results (Fig. 10) and the theoretical results (Fig. 7) are similar. We believe that the difference between the two results is mainly caused by the following reasons.

(i) Due to the existence of tiny bumps on the surface of layers and layup defects such as gaps and blisters, the fluctuations of the pressure and even the contour of each slit-tape can be clearly seen from the experimental results.
(ii) There is a concentration of contact pressure at the left and right sides of the contact zone, which is a feature of the contact of cylindrical body [20], as can be seen from Fig. 9(a)(b)(d). However, this is not considered in the model since the spatial problem is simplified into a plane one.
(iii) The pressure measurement film itself has a measurement error of 0.06 MPa. And the motion error of the AFP machine is around 0.8 mm, leading to a difference between ${}^{Base}\boldsymbol{T}_H$ and ${}^{Base}\boldsymbol{T}_{Pj}$ in Eq. (1).

Given the above aspects, it can be considered that the model is effective.

4.3. Additional AFP experiments

Around path point P_3, the area of the left and right sides of the contact zone was not subjected to sufficient pressure, resulting in low tack level, and the number of layup defects may increase [5,26,27]. In order to understand the practical value of the model, 16-tows placement experiment was carried out along path l, as shown in Fig. 11 (a). The layup speed, compaction force and power of the infrared heater were set as 30 mm/s, 600 N and 120 W, respectively.

After the placement, small wrinkles appeared at the 1st, 2nd and 16th slit-tapes near point P_3, as shown in Fig. 11(b). Moreover, the three slit-tapes were not even sticked to the previous layers. The process conditions (except for compaction pressure) of the all 16 slit-tapes

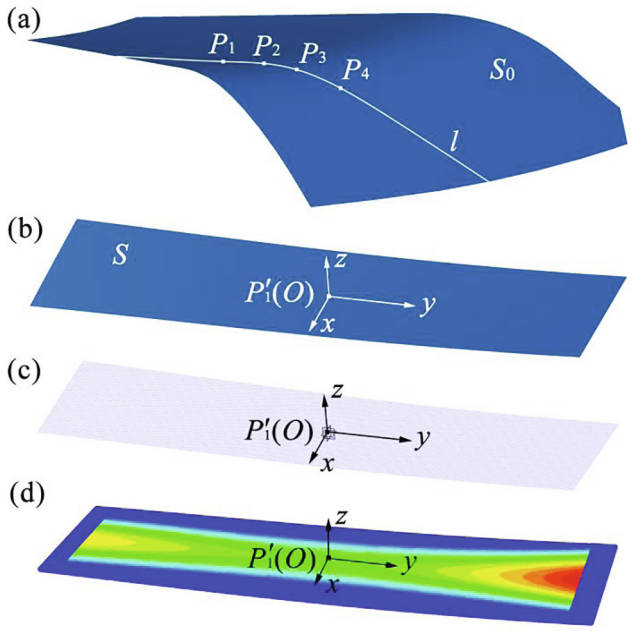

Fig. 6. (a) The surface S_0 of the fifth layer, and the path points P_1, P_2, P_3, P_4 of the path l; (b) the surface S around point P_1' after appropriate cut of S_0; (c) point cloud $\{A_0\}$; (d) compaction pressure distribution around P_1.

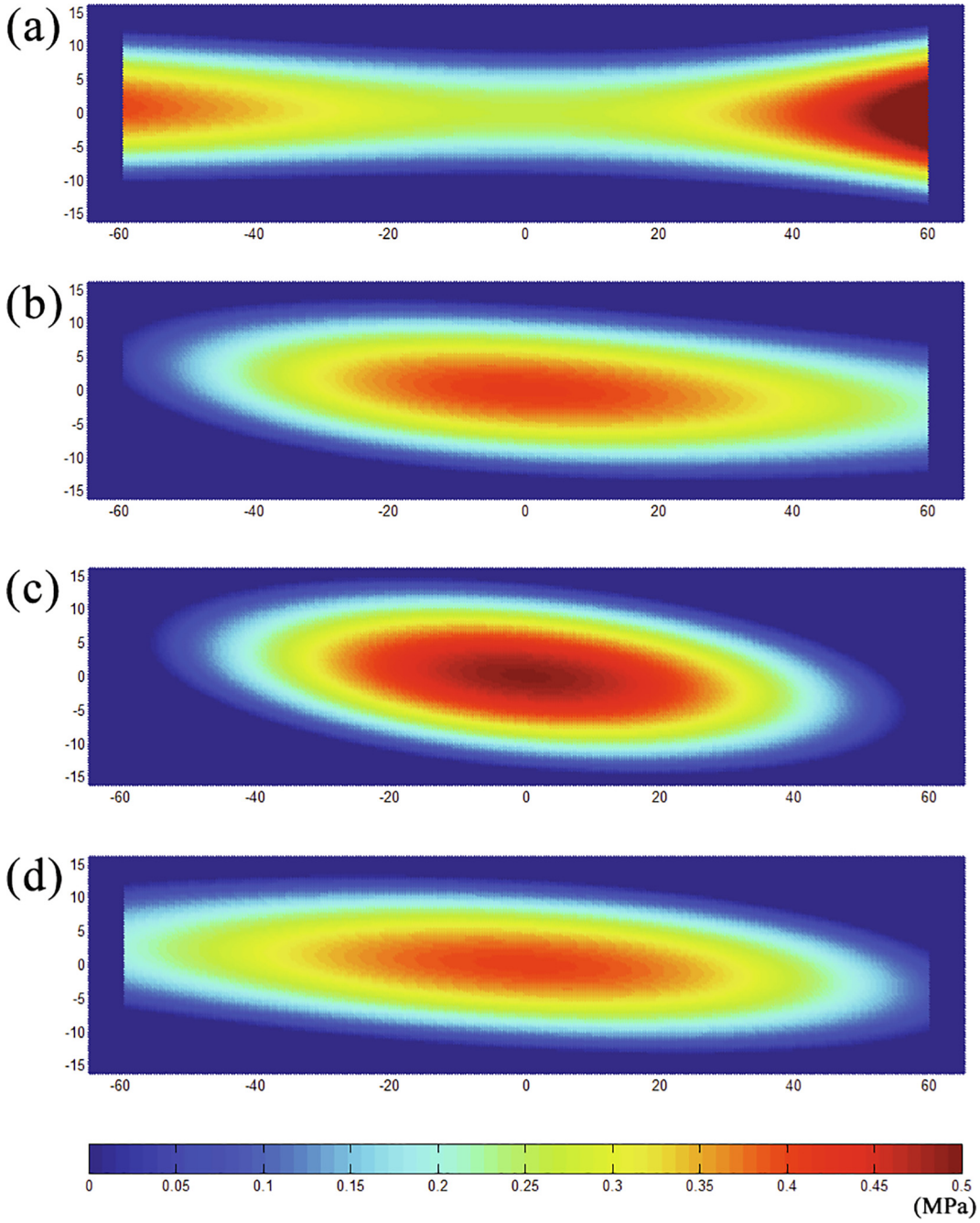

Fig. 7. Numerical calculation results of the compaction pressure distribution around path point: (a) P_1; (b) P_2; (c) P_3; (d) P_4.

are almost the same, thus it seems that the wrinkles and the low tack strength are related to insufficient pressure.

Since the mold surface here is convex and there is no steering, the defects were not obvious. However, for small steering radius, the wrinkles will be more obvious if the pressure is low. And for concave mold, one component of the tension in the slit-tapes is a peeling force, which weakens the pressure and may cause bridgings. In a word, the model can be used to predict the layup defects and layup quality, combining with the shape of mold surface.

Furthermore, according to Eq. (5), the pressure distribution can be improved by selecting appropriate compaction roller: rollers with smaller hardness, length and inner radius, and with larger out radius are better. In addition, reducing the number of slit-tapes before AFP is another way to improve pressure distribution. Moreover, means such as increasing layup temperature and decreasing layup speed can be taken to compensate for the impact of insufficient pressure.

5. Conclusion

The compaction pressure distribution in AFP is an important process parameter, but received little attention. In this paper, after two simplifications, a model of compaction pressure distribution for layup onto irregular curved mold surface is established by analyzing the contact deformation and contact stress between the compaction roller and prepreg layers. Two unknown parameters in the model are fitted by finite element simulation. And the through-thickness modulus of prepreg is obtained by compaction tests. Based on the model, a numerical algorithm for calculating compaction pressure distribution in the

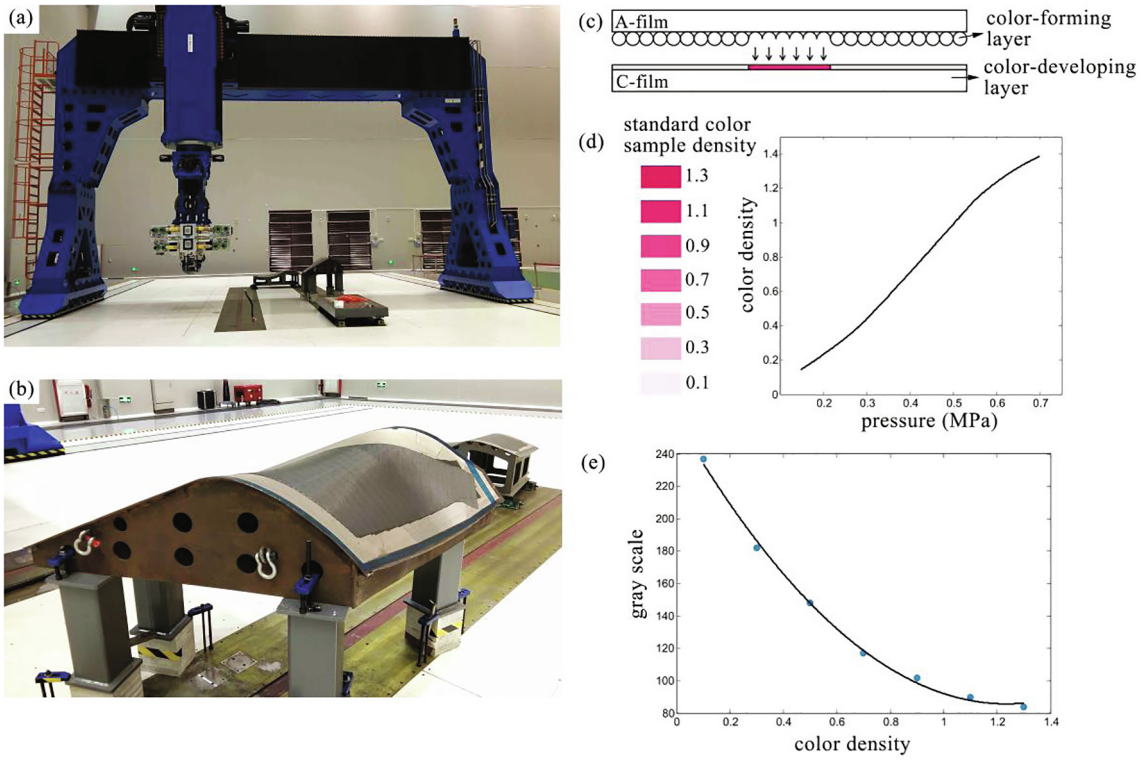

Fig. 8. Experimental setup and pressure measurement film: (a) the 16-tow six-axis gantry AFP machine; (b) the winglet mold; (c) the principle of pressure measurement for the pressure measurement film; (d) the corresponding relationship between pressure and color density; (e) the fitting result of relationship between color sample density and gray scale.

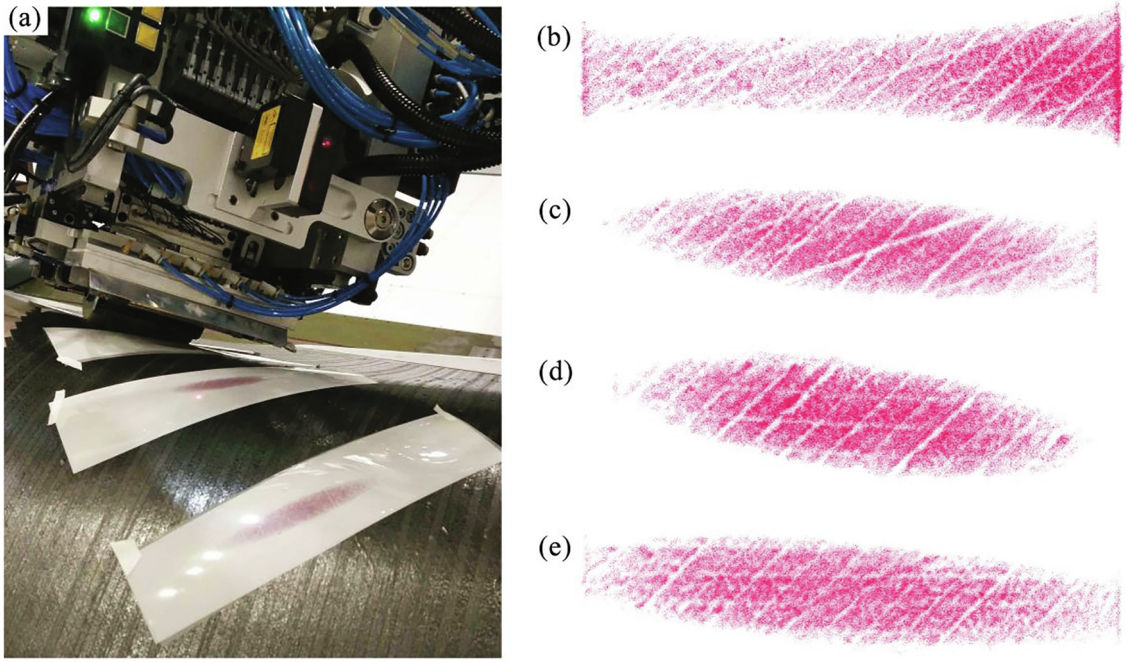

Fig. 9. (a) Compaction pressure distribution measurement experiment; (b) color density distribution on the pressure measurement film after the pressure around point P_1; (c) around P_2; (d) around P_3; (e) around P_4.

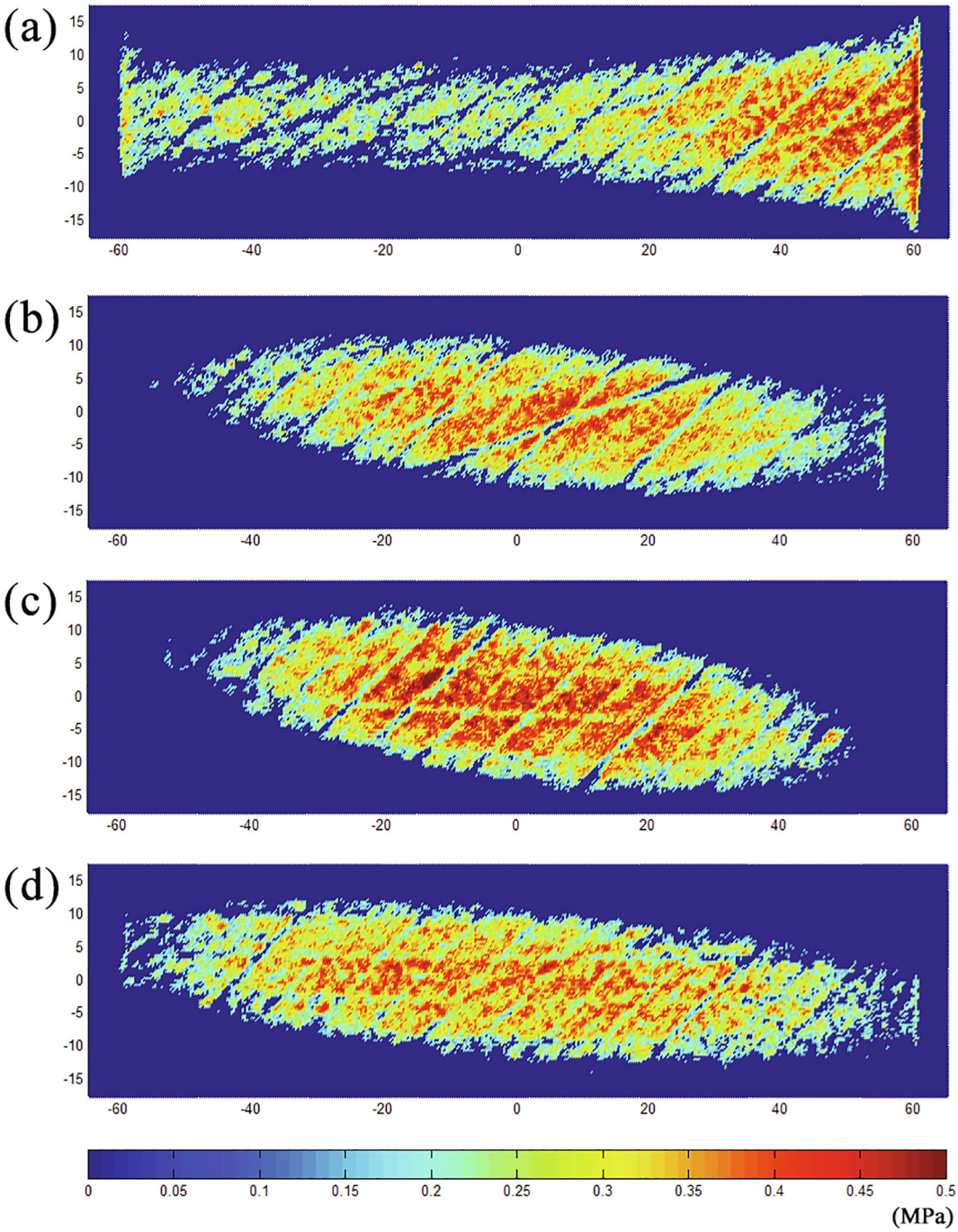

Fig. 10. Experimental results of the compaction pressure distribution around: (a) P_1; (b) P_2; (c) P_3; (d) P_4.

whole AFP process is proposed, and the pressure distribution around four path points of a winglet mold is obtained by the algorithm. In addition, pressure measurement experiment was carried out and the compaction pressure distribution around the four path points was obtained by pressure measurement film. Moreover, additional AFP experiment was preformed to understand the practical value of the model.

Combining with the shape of mold surface and placement paths, the model can be used to predict the pressure distribution in the whole AFP process. With the pressure distribution, the layup defects and layup quality can be better analyzed. In addition, the model provides a basis for selecting appropriate compaction rollers and determining the number of slit-tapes before placement, and has some practical application value.

Funding

This work was supported by the Fundamental Research Funds for the Central Universities [2019FZA4001].

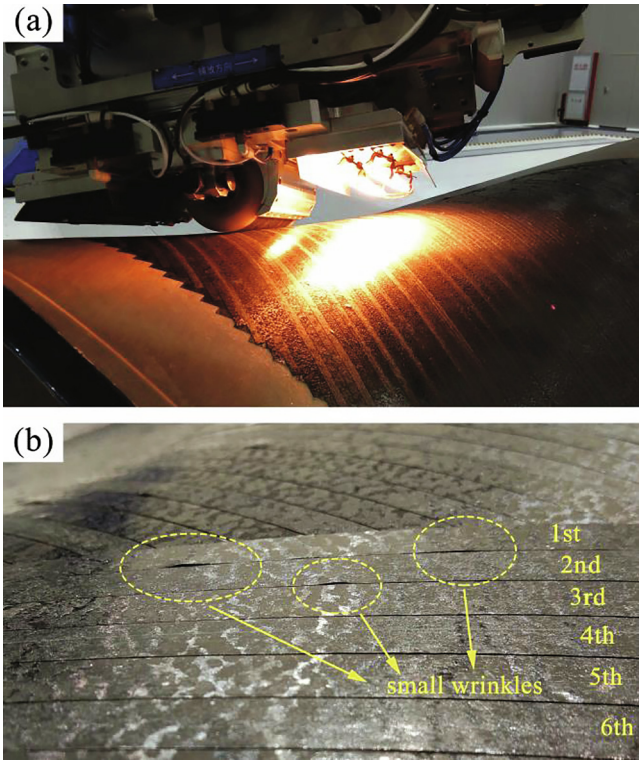

Fig. 11. Additional AFP experiment: (a) 16-tow placement along the path *l*; (b) small wrinkles appeared near point P_3.

Declaration of Competing Interest

The authors declare that they have no known competing financial interests or personal relationships that could have appeared to influence the work reported in this paper.

References

[1] Schmidt C, Schultz C, Weber P, Denkena B. Evaluation of eddy current testing for quality assurance and process monitoring of automated fiber placement. Compos B Eng 2014;56:109–16.
[2] Rouhi M, Ghayoor H, Hoa SV, Hojjati M. Multi-objective design optimization of variable stiffness composite cylinders. Compos B Eng 2015;69:249–55.
[3] Rajan S, Sutton MA, Wehbe R, Tatting B, Gürdal Z, Kidane A, et al. Experimental investigation of prepreg slit tape wrinkling during automated fiber placement process using StereoDIC. Compos B Eng 2019;160:546–57.
[4] Croft K, Lessard L, Pasini D, Hojjati M, Chen J, Yousefpour A. Experimental study of the effect of automated fiber placement induced defects on performance of composite laminates. Compos A Appl Sci Manuf 2011;42:484–91.
[5] Bakhshi N, Hojjati M. Effect of compaction roller on layup quality and defects formation in automated fiber placement. J Reinf Plast Compos 2019;0731684419868845.
[6] Lukaszewicz D-H-J-A, Ward C, Potter KD. The engineering aspects of automated prepreg layup: History, present and future. Compos B Eng 2012;43:997–1009.
[7] Crossley RJ, Schubel PJ, Warrior NA. The experimental determination of prepreg tack and dynamic stiffness. Compos A Appl Sci Manuf 2012;43:423–34.
[8] Dubois O, Le C, Béakou A. Experimental analysis of prepreg tack. Exp Mech 2010;50:599–606. https://doi.org/10.1007/s11340-009-9236-7.
[9] Denkena B, Schmidt C, Völtzer K, Hocke T. Thermographic online monitoring system for Automated Fiber Placement processes. Compos B Eng 2016;97:239–43.
[10] Qureshi Z, Swait T, Scaife R, El-Dessouky HM. In situ consolidation of thermoplastic prepreg tape using automated tape placement technology: potential and possibilities. Compos B Eng 2014;66:255–67.
[11] Aized T, Shirinzadeh B. Robotic fiber placement process analysis and optimization using response surface method. Int J Adv Manuf Technol 2011;55:393–404.
[12] Sonmez FO, Akbulut M. Process optimization of tape placement for thermoplastic composites. Compos A Appl Sci Manuf 2007;38:2013–23.
[13] Khan MA, Mitschang P, Schledjewski R. Parametric study on processing parameters and resulting part quality through thermoplastic tape placement process. J Compos Mater 2013;47:485–99.
[14] Lamontia MA, Gruber MB, Waibel BJ, Cope RD, Hulcher AB. Conformable compaction system used in automated fiber placement of large composite aerospace structures. In: 23rd SAMPE EUROPE Conference, Paris; 2002, p. 9–11.
[15] Lichtinger R, Lacalle J, Hinterhölzl R, Beier U, Drechsler K. Simulation and experimental validation of gaps and bridging in the automated fiber placement process. Sci Eng Compos Mater 2015;22:131–48.
[16] Zhao C, Xiao J, Huang W, Huang X, Gu S. Layup quality evaluation of fiber trajectory based on prepreg tow deformability for automated fiber placement. J Reinf Plast Compos 2016;35:1576–85.
[17] Cheng J, Zhao D, Liu K, Wang Y, Chen H. Modeling and impact analysis on contact characteristic of the compaction roller for composite automated placement. J Reinf Plast Compos 2018;37:1418–32.
[18] Sonmez FO, Hahn HT. Analysis of the on-line consolidation process in thermoplastic composite tape placement. J Thermoplast Compos Mater 1997;10:543–72.
[19] Jiang J, He Y, Ke Y. Pressure distribution for automated fiber placement and design optimization of compaction rollers. J Reinf Plast Compos 2019;38:860–70.
[20] Johnson KL. Contact mechanics. Cambridge University Press; 1985.8..
[21] ISO 7743:2017(E) Rubber, vulcanized or thermoplastic — Determination of compression stress-strain properties
[22] Peng X, Shu Z, Du T, Xu Q. Peel simulating and test verification of prepreg based on laying process. Hangkong Xuebao/Acta Aeronaut Astronaut Sin 2018;39..
[23] Gent AN. Engineering with rubber: how to design rubber components. 3rd ed. München: Carl Hanser Verlag GmbH & Co. KG; 2012.
[24] Peng X. Quality characterization and regulation of prepreg tow steering based on automatic placement process Master thesis. Zhejiang University; 2019.
[25] Lukaszewicz D-H-J-A, Potter K. Through-thickness compression response of uncured prepreg during manufacture by automated layup. Proc Inst Mech Eng Part B: J Eng Manuf 2012;226:193–202.
[26] Bakhshi N, Hojjati M. An experimental and simulative study on the defects appeared during tow steering in automated fiber placement. Compos A Appl Sci Manuf 2018;113:122–31.
[27] Matveev MY, Schubel PJ, Long AC, Jones IA. Understanding the buckling behaviour of steered tows in Automated Dry Fibre Placement (ADFP). Compos A Appl Sci Manuf 2016;90:451–6.